Cross-Beam Energy Transfer Saturation by Ion Heating

A. M. Hansen, K. L. Nguyen, D. Turnbull, B. J. Albright, R. K. Follett, R. Huff, J. Katz, D. Mastrosimone, A. L. Milder, L. Yin, J. P. Palastro, and D. H. Froula

Phys. Rev. Lett. **126**, 075002 — Published 19 February 2021

DOI: 10.1103/PhysRevLett.126.075002

Cross-Beam Energy Transfer Saturation by Ion Heating

A. M. Hansen,[1,2] K. L. Nguyen,[1,2] D. Turnbull,[1] B. J. Albright,[3] R. K. Follett,[1] R. Huff,[1] J. Katz,[1] D. Mastrosimone,[1] A. L. Milder,[1,2] L. Yin,[3] J. P. Palastro,[1] and D. H. Froula[1,2]

[1]*Laboratory for Laser Energetics, University of Rochester, 250 East River Road, Rochester New York 14623, USA*

[2]*Department of Physics and Astronomy, University of Rochester, Rochester New York 14623, USA*

[3]*Los Alamos National Laboratory, Los Alamos, New Mexico 87545, USA*

(Dated: January 21, 2021)

Cross-beam energy transfer (CBET) saturation by ion heating was measured in a gas-jet plasma characterized using Thomson scattering. A wavelength-tunable ultraviolet (UV) probe laser beam was interacted with four intense UV pump beams to drive large-amplitude ion-acoustic waves. For the highest-intensity interactions, the power transferred to the probe laser dropped, demonstrating ion-acoustic wave saturation. Over this time, the ion temperature was measured to increase by a factor of 7 during the 500-ps interaction. Particle-in-cell simulations show ion trapping and a subsequent ion heating consistent with measurements. Linear kinetic CBET models were found to agree well with the observed energy transfer when the measured plasma conditions were used.

In laser-driven inertial confinement fusion (ICF), high-intensity lasers are used to drive capsules that reach pressure and temperature conditions required for nuclear fusion [1]. This requires multiple overlapping laser beams to propagate through plasmas surrounding the fusion capsule. The plasma mediates energy transfer between the laser beams, which can disrupt the energy coupling and/or cause irradiation nonuniformity [2, 3]. To account for this cross-beam energy transfer (CBET), linear models have been implemented in the hydrodynamic codes used to simulate ICF experiments [4, 5]. The ability to predict this transfer of energy is critical to the success of all laser-driven ICF concepts.

The power transfer between beams is sensitive to the plasma conditions. Figure 1(a) highlights the sensitivity of CBET to ion temperature, underscoring the importance of accurate models in determining the plasma conditions in order to predict its effect on implosions. Uncertainties in plasma conditions have led to challenges in isolating errors between the modeling and experimental observables [6], which has made it difficult to understand the limitations of the linear CBET theory [7].

Particle-in-cell simulations have suggested that when the ion-acoustic waves are driven to large amplitude, nonlinear effects will modify the energy transfer resulting in deviations from linear CBET theory [8, 9]. Early experiments seemed to corroborate this picture, suggesting that nonlinear physics was required to model the interactions, but these experiments relied primarily on hydrodynamic modeling to determine the plasma conditions [10, 11] and due to the uncertainties in plasma conditions an understanding of the saturation physics was elusive. The most complete studies to date have used Thomson-scattering from electron-plasma waves to measure the electron temperature and density, while simultaneously measuring the energy transfer [12, 13]. At small ion-acoustic wave amplitudes ($\delta n/n_e < 1\%$), these experiments were well modeled by linear CBET theory, but for larger ion-acoustic wave amplitudes, discrepancies from linear theory were evident [14]. Theory and simulations have recently suggested that energy dissipation of the large amplitude ion-acoustic waves could lead to ion heating and therefore reduce the power transfer [15], but no direct experimental evidence has been established.

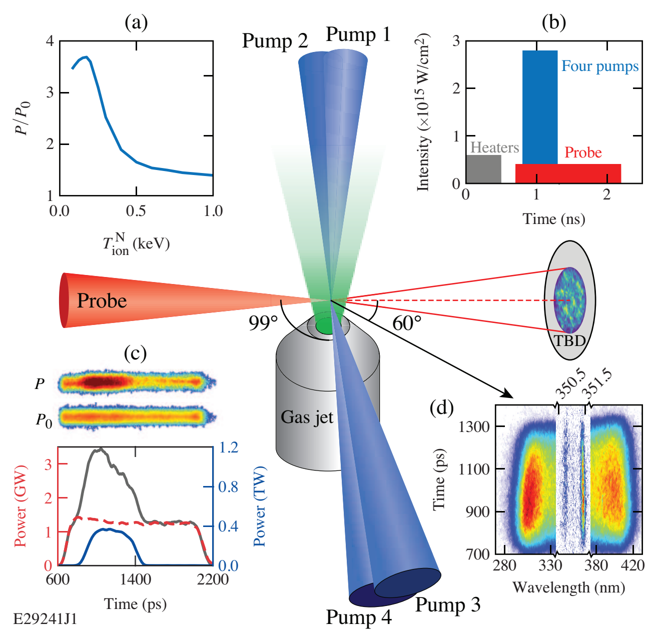

FIG. 1. (a) The ratio of the output power (P) to the incident power (P_0) of the probe beam was calculated using a linear kinetic CBET model for the conditions of these experiments over a range of nitrogen ion temperatures. (b) The total laser intensity, pulse shapes, and beam timings for each of the beam groups. (c) Transmitted beam diagnostic (TBD) data showing the input- (dashed red curve) and output- (solid black curve) probe and pump (blue curve) powers. (d) Time-resolved Thomson-scattering data showing the electron-plasma and ion-acoustic wave spectra of a pump beam with minimal ion heating.

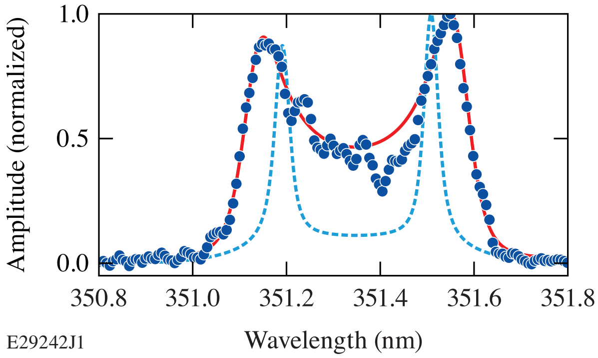

FIG. 2. The ion-acoustic wave spectrum measured (points) after the CBET pump beams turned off ($\sim$ 1600 ps). A calculated spectrum (red curve) is in excellent agreement with the measured spectrum for the plasma conditions: $T_e = 450$ eV, $T_{ion}^{H} = 750$ eV, and $T_{ion}^{N} = 900$ eV. The calculated spectrum (blue dashed curve) for the ion temperatures with no ion heating ($T_e = 450$ eV, $T_{ion}^{H} = 120$ eV, $T_{ion}^{N} = 120$ eV).

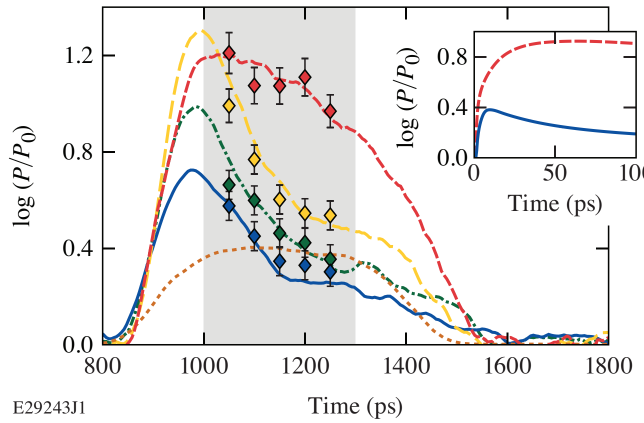

FIG. 3. The power transferred into the probe beam for four different initial probe beam intensities [0.1×10^{14} W/cm^2 (red short dashed curve), 0.9×10^{14} W/cm^2 (yellow long dashed curve), 2.0×10^{14} W/cm^2 (green dashed-dotted curve), 4.1×10^{14} W/cm^2 (blue solid curve)]. The pulse shape of the pump beams (orange dashed curve) is shown. The energy transfer calculated using kinetic linear theory for the measured plasma conditions (diamonds). The inset shows VPIC simulated probe beam amplification corresponding to the lowest (red dashed curve) and highest (blue solid curve) experiment probe intensities.

In this Letter, we present the first measurements of the saturation of cross-beam energy transfer by ion heating. At the highest intensities studied (4×10^{14} W/cm^2), saturation of CBET was observed through a significant reduction (factor of 3) in relative power gained compared with the power gained at the lowest probe intensity (0.1×10^{14} W/cm^2). Simultaneous Thomson-scattering measurements from the ion-acoustic and electron-plasma waves showed a factor of 7 increase in the ion temperature for the highest-intensity CBET interactions. The measured time-dependent energy transfer was in excellent agreement with linear CBET calculations for all intensities studied when accounting for the measured plasma conditions. Vector particle-in-cell (VPIC) [16, 17] simulations demonstrate the mechanism of ion heating and qualitatively reproduce the experiments. The simulations showed ion trapping over the first $\sim$10 ps generating high-velocity ions near the phase velocity of the driven ion-acoustic waves. Over the next $\sim$100 ps, these hot ions thermalized with the background plasma, increasing the ion temperature. For these conditions, the nonlinear physics leads to an increase in plasma temperature, which limits the CBET to the linear regime. These results highlight not only the importance of plasma conditions in accurately determining CBET, but also the importance of including the feedback of CBET heating on ion temperature in hydrodynamic modeling.

The experiment was performed on the OMEGA [18] laser-plasma interaction platform. Figure 1 illustrates the experimental configuration that consisted of a gas-jet system that produced a gas plume, which was heated by nine 500-ps long ultraviolet (UV) beams. The gas jet used a Mach 2.6, 2-mm exit diameter nozzle (M3-2.0 designation), which was $\sim$2 mm away from target chamber center (TCC). The target gas was a mixture of 45% nitrogen and 55% hydrogen to approximately reproduce the ion-acoustic wave damping from typical ICF experiments. The heater beams used large phase plates [850 μm full-width half-maximum (FWHM)] to produce a uniform plasma with a $\sim$1.5 mm diameter plateau at a density of $n_e = 8 \times 10^{19}$ cm^{-3} [19].

To avoid overlap between the heater beams and CBET experiments, the pump and probe beams were turned on 800 ps into the experiment [Fig. 1(b)], and crossed at an angle of 99° at TCC. The probe beam used the Tunable Omega Port-9 (TOP9) laser [20], which was wavelength tunable over $\sim$3 nm around the pump beams' wavelength of 351.11 nm. The resonant wavelength of the probe beam (351.40 nm) was used for all experiments and was determined by maximizing the energy transfer while scanning its wavelength; the probe beam was held at the lowest intensity. The probe beam used a phase plate, which created a 160-μm-diam FWHM spot at TCC. The 1.5-ns flattop pulse duration and 125-J maximum energy of the probe beam generated a maximum intensity of 4×10^{14} W/cm^2. The pump beams used phase plates that created elliptical spots with a minor radius of 110 μm and a major radius of 160 μm at half maximum. The 500-ps flattop pulse duration with $\sim$180 J per beam delivered a single-beam area-averaged intensity of $\sim 7 \times 10^{14}$ W/cm^2. The minor axis of the pump beam was aligned nearly parallel to axis of the probe beam, limiting their interactions to $L \sim 220$ μm. The pump and probe beams had linear polarizations, which were aligned for an S-polarized CBET interaction.

The time-resolved power in the probe laser was measured with the transmitted beam diagnostic (3ω TBD) [21]. The 3ω TBD collected the light of the probe beam after its interaction with the pump beams on a spectralon sheet (diffuser), which was sampled by a two-camera system; one time-integrated space-resolved system measured the transmitted energy and the other spectrally and temporally resolved system measured the power. The incident probe beam energy was measured using an absolutely calibrated calorimeter. A beam pickoff prior to the target chamber measured the input probe beam pulse shape. A streak camera coupled to a spectrometer spectrally and temporally resolved both the incident and transmitted probe beam with a temporal resolution of 50 ps and a spectral resolution of 0.01 nm [Fig. 1(c)].

The plasma conditions in the experiment were measured with the Thomson-scattering system (TSS) [Fig. 1(d)] [22]. The TSS collected light from a $\sim$160 μm $\times$ 60 μm $\times$ 60 μm volume at TCC and transported it to a suite of streak cameras coupled to spectrometers. The light was collected $\sim$60° from the probe beam axis by an f/10 telescope, which directed the light to the 1-m and 1/3-m spectrometer-streak camera pairs providing a measurement of the ion-acoustic wave (IAW) and electron-plasma wave (EPW) spectrum. The temporal resolutions of these measurements were $\sim$50 ps and the spectral resolutions were 0.02 nm and 0.5 nm for the IAW and EPW systems respectively.

Figure 2 shows the measured ion-acoustic wave spectrum (blue points) from the highest-intensity CBET experiments. Comparing the calculated ion-acoustic wave spectrum for no ion heating to the measured spectrum after CBET ($\sim$1600 ps) shows a significant difference in the widths of the ion-acoustic wave features. This increased width is a direct result of a significant change in the ion temperature over the time CBET was active (T_{ion}^{N} = 120 eV $\rightarrow$ 900 eV). This late-time nitrogen ion temperature (T_{ion}^{N} = 900 eV) significantly exceeds the electron temperature (T_e = 450 eV), which was set by inverse bremsstrahlung heating. Prior to the CBET interactions (or for the complete duration of the lowest intensity interaction experiment), equilibration of the laser-heated electrons with the ions is the only mechanism for ion heating. The Thomson-scattering spectra were numerically calculated using the non-Maxwellian form of the standard multiple-species collisionless spectral density function [23, 24].

Figure 3 shows the amplification of the probe beam due to CBET at four initial probe intensities. The fact that the power ratio P/P_0 decreases with increasing probe intensity for minimal pump depletion suggests nonlinear saturation. Furthermore, every probe beam intensity greater than 0.1 $\times$ 10^{14} W/cm^2 exhibits a strong time-dependent reduction in amplification. For the three highest initial probe beam intensities, the amplification started high ($\sim$1000 ps), but decreased over time before plateauing toward the end of the pump pulse ($\sim$1300 ps).

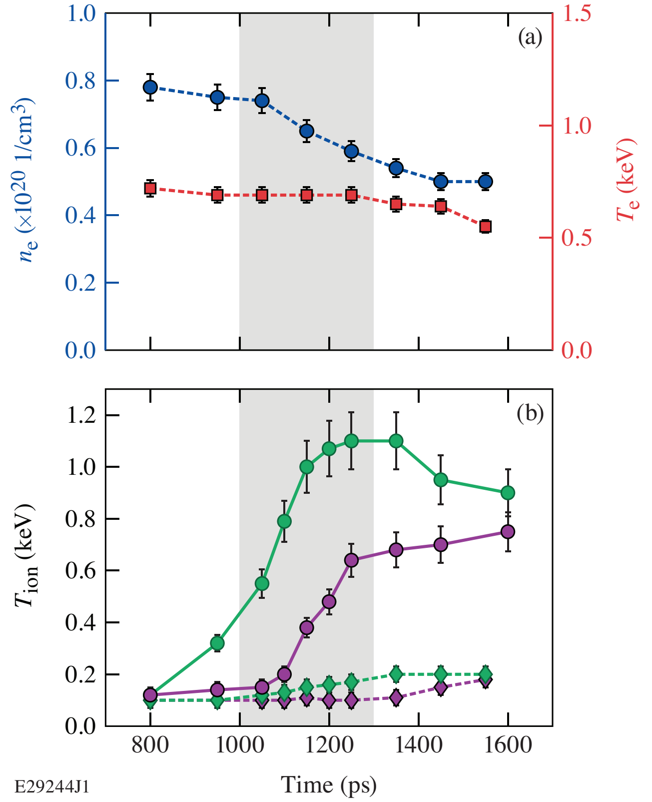

FIG. 4. The plasma conditions for the (a) electrons (b) and ions measured from the Thomson-scattering spectrum. The ion temperatures for nitrogen (green points) and hydrogen (purple points) are shown for two shots corresponding to the lowest (I$_{probe}$=0.1 $\times$ 10^{14} W/cm^2) (diamonds) and highest (I$_{probe}$=4.1 $\times$ 10^{14} W/cm^2) (circles) probe beam intensities.

Figure 4 shows the plasma conditions measured by Thomson scattering. The time-resolved electron density and electron temperature conditions measured in the CBET volume over the duration of the pump beams indicate a nearly constant electron temperature and a slowly decreasing electron density throughout the experiment [Fig. 4(a)]. These conditions were nearly identical for all CBET experiments. Note that electron distribution functions were found to be non-Maxwellian [13, 24], which was accounted for in Thomson scattering calculations, CBET calculations, and the VPIC simulations by using a super-Gaussian electron distribution function consistent with inverse bremsstrahlung heating [25]. The shaded region shows the period when CBET energy transfer was most active.

Figure 4(b) shows the evolution of the ion temperatures. The ion temperatures for the lowest-intensity shot remain relatively low and only gradually increase over time from $\sim$120 eV to $\sim$200 eV as the ion temperature begins to equilibrate with the electron temperature. The ion temperature for the highest-intensity shot also starts

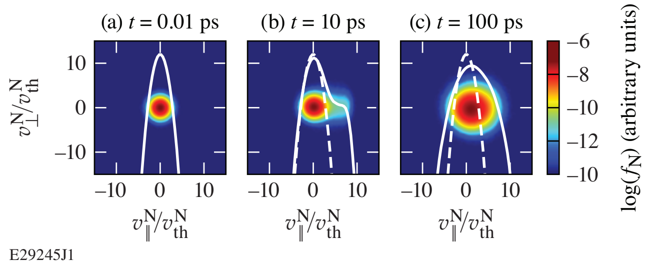

FIG. 5. VPIC simulations of a plasma prepared identically to the experimental plasma show the 2-D nitrogen ion velocity distribution functions for a high probe beam intensity CBET interaction at three time steps; (a) T = 0.01 ps, (b) T = 10 ps, (c) and T = 100 ps. The x axis (y axis) of each subplot is the velocity parallel (perpendicular) to the excited ion wave normalized to the initial nitrogen thermal velocity. A line shows the log of the 1-D velocity distribution parallel to the excited ion wave (solid line) compared to the initial distribution (dashed line).

low ($\sim$120 eV), but rapidly increases over the time when significant energy transfer occurs in the grey shaded region. In both cases the nitrogen ions heat faster than the hydrogen ions and the two species reach an approximate thermal equilibrium near the end of the measurement. Ion heating follows necessarily from conservation of energy and momentum in the CBET interaction [26] and the fact that it is more significant at high incident probe power is consistent with the larger amount of power transferred. The thermal energy partitioning between the nitrogen and hydrogen ions is consistent with collisional heating where the N-N (H-N) collision time is $\sim$5 ps ($\sim$33 ps) for $\sim$150 eV ion temperatures.

Using the measured plasma conditions (Fig. 4), the linear kinetic CBET power amplification was calculated (Fig. 3) [15]. These CBET calculations are in excellent agreement with the measurements at all times and across all probe intensities tested. The time-dependent decreasing amplification at the lowest probe beam intensity (0.1×10^{14} W/cm^2) was due to the modest decrease in plasma density as a result of the hydrodynamic expansion of the plasma. The more-dramatic decrease in amplification observed for the higher-intensity shots was a direct result of the increase in ion temperature over the course of the CBET. As the ions were heated, the IAW dispersion evolved along a new branch with increased frequency at the wavenumber determined by the crossing angle. Because the driving frequency was fixed, the driven IAW was no longer at a resonant frequency, which increased the wave damping and saturated CBET. Probe beam propagation studies at the highest intensity were performed to exclude forward stimulated Raman scattering and self-focusing as apparent saturation mechanisms [27]; energy transmission and spectral measurements indicated no energetically significant instability.

Figure 5 shows the normalized 2-D nitrogen ion velocity distribution functions calculated from VPIC simulations of a high probe beam intensity single-pump-beam CBET experiment with initial plasma conditions matching the experimental plasma. Initially the nitrogen ions are at a low temperature ($T^N_{ion} = 150$ eV) and the velocity distribution function was Maxwellian along both of the spatial dimensions defined to be perpendicular (y axis) and parallel (x axis) to the driven ion-acoustic wave vector. At 10 ps [Fig. 5(b)], the large ion-acoustic waves driven by CBET have trapped and accelerated the nitrogen ions to the phase velocity of the wave ($v_{ph}/v^N_{th} \sim 4.3$ is the ratio of the ion-acoustic phase velocity to the nitrogen thermal velocity). As the accelerated ions collide with the bulk of the ions, the overall ion velocity distribution function was heated and nearly reaches a super-Gaussian shape after 100 ps with a higher temperature of $\sim$720 eV [Fig. 5(c)]. The electron velocity distributions remain largely unaffected due to slow temperature equilibration rate between the ions and electrons. Figure 3(inset) shows the probe beam amplification corresponding to high and low simulated probe beam intensities. IAW breakup and nonlinear ion trapping effects that led to ion heating were observed on short-transient time scales ($\sim$10 ps), but the nonlinear dynamics were not significant in saturating CBET on long time scales ($\sim$100 ps) [9, 27].

VPIC is a relativistic, electromagnetic particle-in-cell code with a binary collision model [28] that recovers the Landau form of inter-particle collisions for weakly coupled plasmas. The 2-D simulation shown in Fig. 5 used a domain size of 138 μm $\times$ 108 μm, cell size equal to the Debye length, and 512 computational particles/cell/species. The speckled laser beams were generated as in Ref. [27] with diameters of 68 μm, polarized out of the plane, and launched at an angle 99° from one another. The initial plasma conditions were chosen to match the experiment, the ions were Maxwellian ($T_{ion} = 150$ eV) and the electrons super-Gaussian [25] with $m = 3$ ($T_e = 600$ eV). The field boundaries were absorbing and the particle boundaries were refluxing with Maxwellian (super-Gaussian) reinjection for ions (electrons).

In summary, the saturation of energy transfer between crossing laser beams due to ion heating was measured. Time-resolved Thomson-scattering measurements indicate an increase in ion temperatures during the CBET interaction. Calculations of the predicted probe beam amplification using linear kinetic CBET theory agree well with the measured amplification when the plasma conditions determined with Thomson scattering were taken into account. The rapid ion heating and resulting CBET saturation qualitatively agrees with models for CBET saturation in indirect-drive ICF experiments [15]. VPIC simulations indicate that at high-probe beam intensities, ion trapping in the driven ion-acoustic wave accelerates ions on short ($\sim$10 ps) time scales. At longer time scales ($\sim$100 ps) the trapped ions heat the bulk of the ion distributions. Although significant nonlinear CBET physics is occurring, it is interesting that linear CBET theory reproduces the measured results when accounting for the instantaneous plasma conditions. However, the plasma conditions are affected by CBET, suggesting that feedback from laser plasma instabilities on hydrodynamics must be accounted for in modeling to accurately predict the energy transfer [3, 15, 29].

This material is based upon work supported by the Department of Energy National Nuclear Security Administration under Award No. DE-NA0003856, the University of Rochester, and the New York State Energy Research and Development Authority.

---

[1] R. Betti and O. A. Hurricane, Nature Physics **12**, 445 (2016).

[2] V. N. Goncharov, T. C. Sangster, P. B. Radha, R. Betti, T. R. Boehly, T. J. Collins, R. S. Craxton, J. A. Delettrez, R. Epstein, V. Y. Glebov, S. X. Hu, I. V. Igumenshchev, J. P. Knauer, S. J. Loucks, J. A. Marozas, F. J. Marshall, R. L. McCrory, P. W. McKenty, D. D. Meyerhofer, S. P. Regan, W. Seka, S. Skupsky, V. A. Smalyuk, J. M. Soures, C. Stoeckl, D. Shvarts, J. A. Frenje, R. D. Petrasso, C. K. Li, F. Seguin, W. Manheimer, and D. G. Colombant, Physics of Plasmas **15** (2008), 10.1063/1.2856551.

[3] D. J. Strozzi, D. S. Bailey, P. Michel, L. Divol, S. M. Sepke, G. D. Kerbel, C. A. Thomas, J. E. Ralph, J. D. Moody, and M. B. Schneider, Physical Review Letters **118**, 1 (2017).

[4] P. Michel, L. Divol, E. A. Williams, S. Weber, C. A. Thomas, D. A. Callahan, S. W. Haan, J. D. Salmonson, S. Dixit, D. E. Hinkel, M. J. Edwards, B. J. MacGowan, J. D. Lindl, S. H. Glenzer, and L. J. Suter, Physical Review Letters **102**, 1 (2009).

[5] I. V. Igumenshchev, W. Seka, D. H. Edgell, D. T. Michel, D. H. Froula, V. N. Goncharov, R. S. Craxton, L. Divol, R. Epstein, R. Follett, J. H. Kelly, T. Z. Kosc, A. V. Maximov, R. L. Mccrory, D. D. Meyerhofer, P. Michel, J. F. Myatt, T. C. Sangster, A. Shvydky, S. Skupsky, and C. Stoeckl, **056314** (2015).

[6] R. K. Kirkwood, B. B. Afeyan, W. L. Kruer, B. J. MacGowan, J. D. Moody, D. S. Montgomery, D. M. Pennington, T. L. Weiland, and S. C. Wilks, Phys. Rev. Lett. **76**, 2065 (1996).

[7] W. L. Kruer, S. C. Wilks, B. B. Afeyan, and R. K. Kirkwood, Physics of Plasmas **3**, 382 (1996).

[8] B. I. Cohen, B. F. Lasinski, A. B. Langdon, and E. A. Williams, Physics of Plasmas **4**, 956 (1997).

[9] L. Yin, B. J. Albright, D. J. Stark, W. D. Nystrom, R. F. Bird, and K. J. Bowers, Physics of Plasmas **26** (2019), 10.1063/1.5111334.

[10] S. H. Glenzer, L. M. Divol, R. L. Berger, C. Geddes, R. K. Kirkwood, J. D. Moody, E. A. Williams, and P. E. Young, Phys. Rev. Lett. **86**, 2565 (2001).

[11] R. K. Kirkwood, J. D. Moody, A. B. Langdon, B. I. Cohen, E. A. Williams, M. R. Dorr, J. A. Hittinger, R. Berger, P. E. Young, L. J. Suter, L. Divol, S. H. Glenzer, and O. L. Landen, Phys. Rev. Lett. **89**, 215003 (2002).

[12] D. Turnbull, C. Goyon, G. E. Kemp, B. B. Pollock, D. Mariscal, L. Divol, J. S. Ross, S. Patankar, J. D. Moody, and P. Michel, Physical Review Letters **118**, 1 (2017).

[13] D. Turnbull, A. Colaïtis, A. M. Hansen, A. L. Milder, J. P. Palastro, J. Katz, C. Dorrer, B. E. Kruschwitz, D. J. Strozzi, and D. H. Froula, Nature Physics **16** (2020), 10.1038/s41567-019-0725-z.

[14] D. Turnbull, A. Colatis, R. K. Follett, J. P. Palastro, D. H. Froula, P. Michel, C. Goyon, T. Chapman, L. Divol, G. E. Kemp, D. Mariscal, S. Patankar, B. B. Pollock, J. S. Ross, J. D. Moody, E. R. Tubman, and N. C. Woolsey, Plasma Phys. Controlled Fusion **60**, 054017 (2018).

[15] P. Michel, W. Rozmus, E. A. Williams, L. Divol, R. L. Berger, R. P. J. Town, S. H. Glenzer, and D. A. Callahan, Phys. Rev. Lett. **109**, 195004 (2012).

[16] K. J. Bowers, B. J. Albright, L. Yin, B. Bergen, and T. J. Kwan, Physics of Plasmas **15** (2008), 10.1063/1.2840133.

[17] K. J. Bowers, B. J. Albright, L. Yin, W. Daughton, V. Roytershteyn, B. Bergen, and T. Kwan, Journal of Physics: Conference Series **180** (2009), 10.1088/1742-6596/180/1/012055.

[18] T. R. Boehly, D. L. Brown, R. S. Craxton, R. L. Keck, J. P. Knauer, J. H. Kelly, T. J. Kessler, S. A. Kumpan, S. J. Loucks, S. A. Letzring, F. J. Marshall, R. L. McCrory, S. F. B. Morse, W. Seka, J. M. Soures, and C. P. Verdon, Opt. Commun. **133**, 495 (1997).

[19] A. M. Hansen, D. Haberberger, J. Katz, D. Mastrosimone, R. K. Follett, and D. H. Froula, Rev. Sci. Instrum **89**, 10C103 (2018).

[20] B. E. Kruschwitz, J. Kwiatkowski, C. Dorrer, M. Barczys, A. Consentino, D. H. Froula, M. J. Guardalben, E. M. Hill, D. Nelson, M. J. Shoup, D. P. Turnbull, L. J. Waxer, and D. Weiner, **1089804**, 3 (2019).

[21] J. Katz, D. Turnbull, B. Kruschwitz, A. Rigatti, R. Rinefierd, and D. Froula, under review Review of Scientific Instruments.

[22] J. Katz, R. Boni, C. Sorce, R. Follett, M. J. S. III, and D. H. Froula, Rev. Sci. Instrum. **83**, 10E349 (2012).

[23] D. H. Froula, S. H. Glenzer, N. C. Luhmann, Jr., and J. Sheffield, *Plasma Scattering of Electromagnetic Radiation: Theory and Measurement Techniques*, 2nd ed. (Academic Press, Amsterdam, 2011).

[24] A. L. Milder, H. P. Le, M. Sherlock, P. Franke, J. Katz,

S. T. Ivancic, J. L. Shaw, J. P. Palastro, A. M. Hansen, I. A. Begishev, W. Rozmus, and D. H. Froula, Physical Review Letters **124** (2020), 10.1103/PhysRevLett.124.025001.

[25] J. P. Matte, M. Lamoureux, C. Moller, R. Y. Yin, J. Delettrez, J. Virmont, and T. W. Johnston, Plasma Physics and Controlled Fusion **30**, 1665 (1988).

[26] J. M. Manley and H. E. Rowe, Proceedings of the IRE , 904 (1954).

[27] L. Yin, B. J. Albright, H. A. Rose, D. S. Montgomery, J. L. Kline, R. K. Kirkwood, P. Michel, K. J. Bowers, and B. Bergen, Physics of Plasmas **20** (2013), 10.1063/1.4774964.

[28] T. Takizuka and H. Abe, Journal of Computational Physics **25**, 205 (1977).

[29] P. Michel, W. Rozmus, E. A. Williams, L. Divol, R. L. Berger, S. H. Glenzer, and D. A. Callahan, Physics of Plasmas **20** (2013), 10.1063/1.4802828.